Supplementary Materials:

Mara Otero-Fernandez [1], **Richard J. Thomas** [2], **Henry Oswin** [3], **Robert Alexander** [1], **Allen Haddrell** [1,*]
and Jonathan P. Reid [1]

Table S1. List of components for the artificial saliva media[2].

Chemical Species	Mol. Wt	Concn (g per 100 mL)
$MgCl_2$	203.21	0.004
$CaCl_2.H_2O$	110.99	0.013
$NaHCO_3$	84.006	0.042
0.2M KH_2PO_4	136.09	2.7218
0.2M K_2HPO_4	174.2	3.484
NH_4Cl	53.49	0.011
KSCN	97.18	0.019
$(NH2)_2CO$	60.06	0.012
NaCl	58.44	0.088
KCl	74.55	0.104
Mucin	N/A	0.3
DMEM	N/A	0.1 mL

Table S2. List of components for the artificial sputum media[1].

Chemical Species	Mol. Wt	Conc (g per 100 mL)
DNA (fish sperm)	N/A	0.4
Mucin	N/A	0.5
L-tyrosine	181.19	0.025
L-cysteine	121.16	0.025
L-alanine	89.09	0.025
L-arginine	174.2	0.025
L-aspartic acid	133.1	0.025
L-glutamic acid	147.1	0.025
L-glutamine	146.1	0.025
L-glycine	75.07	0.025
L-histidine	155.2	0.025
L-isoleucine	131.2	0.025
L-leucine	131.2	0.025
L-lysine.HCl	182.6	0.025
L-methionine	149.2	0.025
L-phenylalanine	165.19	0.025
L-proline	115.1	0.025
L-serine	105.1	0.025
L-threonine	119.1	0.025
L-tryptophan	204.23	0.025
L-ornithine	168.62	0.025
L-valine	117.1	0.025
DTPA	393.55	0.0059
NaCl	58.44	0.5
KCl	74.55	0.22

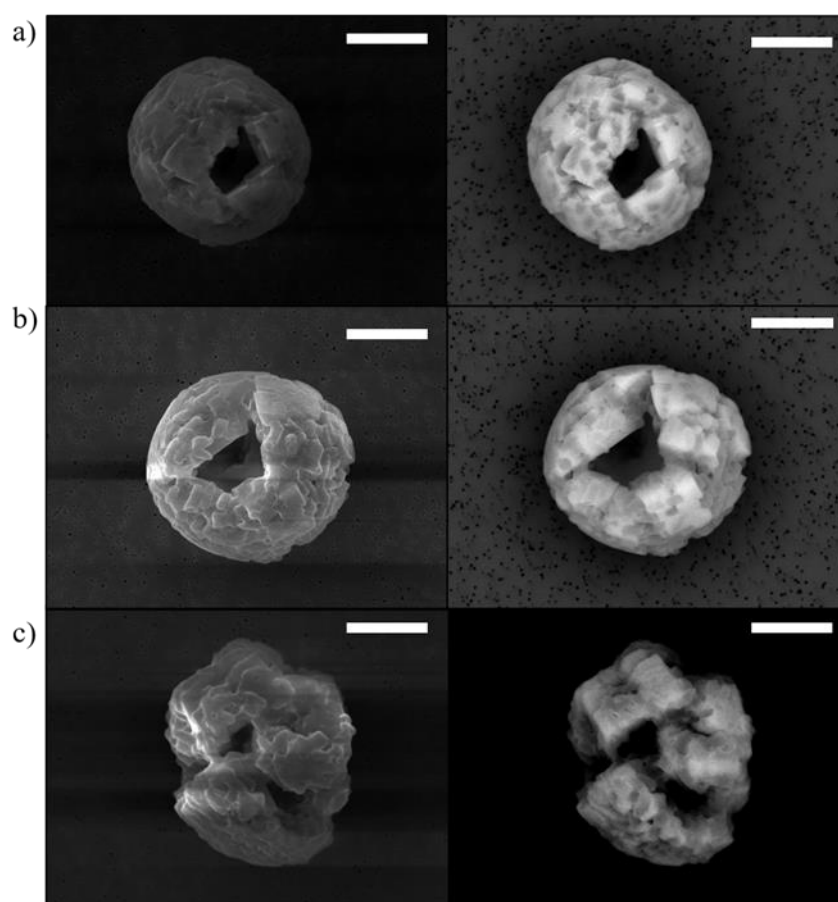**Changes in Morphology of Bioaerosol Droplets Across a wide range of RHs**

Figure S1. SEM images of *E. coli* MRE-162 cells at a concentration of ~10^9 CFU mL^{-1} levitated in PBS droplets at (**a**) 10%RH, (**b**) 30% RH and (**c**) 50% RH. Scale bars represent 5 μm.

Measurements of Physicochemical Properties of Surrogate Respiratory Aerosol with the CK-EDB

To accurately capture the interconnection of airborne viability measurements with measurements of different physicochemical properties, both measurements must ideally be done in parallel with particles of the same size, over the same timescales and using the same method for aerosol generation. To that aim, the hygroscopic properties and evaporation dynamics must be measured for droplets chemically and physically identical to those where biological decay is measured.

The hygroscopic properties of artificial respiratory droplets (e.g., artificial saliva and sputum) were characterized (Figure S2). The relationships between solute composition with the ambient RH for droplets made of representative respiratory secretions are compared with previously published hygroscopicity measurements for common microbiological media (e.g. LB broth and PBS solution droplets)[15] and model predictions for NaCl from E-AIM (extended aerosol inorganics model).[13]

In general, aerosol droplets containing a large solute fraction of inorganic compounds, such as PBS and NaCl, have higher hygroscopicity than droplets containing a significant organic solute fraction. Similar hygroscopic responses are inferred for both LB broth (60% of the mass arising from organic components) and artificial sputum (80% of organics by mass). The artificial saliva droplets are the least hygroscopic of the series despite high salt content (approximately 95% of salts by mass, Table S1). This could be explained by the presence of organic compounds in the recipe, making them absorb less water than the pure salt compositions. These results are consistent with our previous report of the hygroscopicity of surrogate deep lung fluid and artificial saliva.[16] Once the hygroscopicity is determined, it is possible to assess the impact of solute concentration

changes on the survival of the microbial components hosted within the aerosol. For instance, considering an artificial saliva droplet, its solute weight percentage will change from 15% to 50% when the ambient RH decreases from 90% to 50%. This dramatic change in concentration can be expected to influence microbial health.
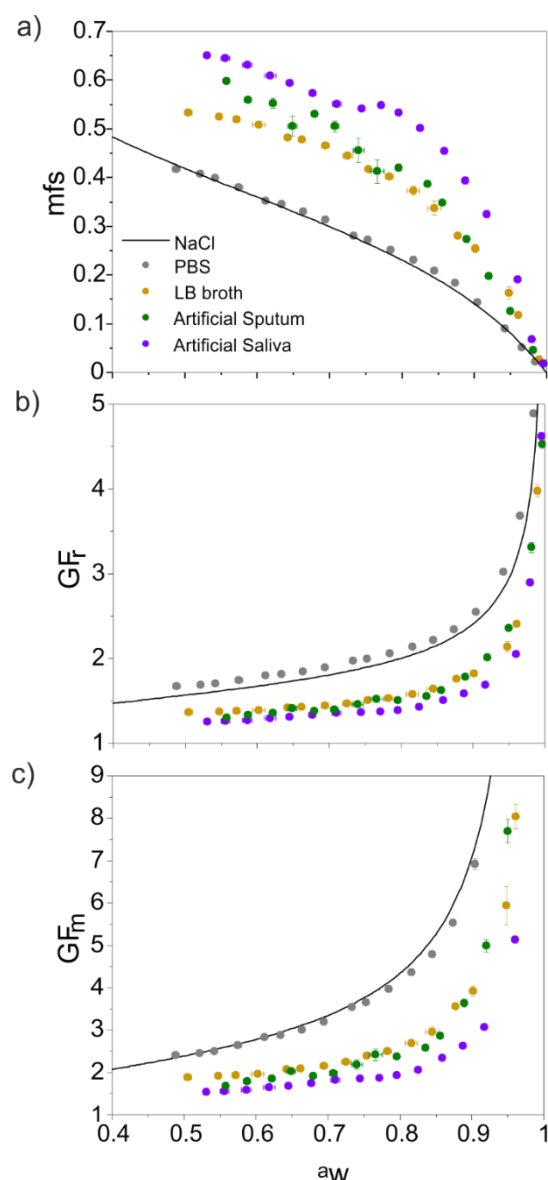

Figure S2. Hygroscopic response of various droplet solutions (e.g. PBS, LB broth, artificial saliva and artificial sputum) as a function of droplet water activity (a_w), equivalent to the gas-phase RH, presented in terms of (**a**) mass fraction of solute (MFS), (**b**) mass growth factor (GF_m) and (**c**) and radial growth factor (GF_r). The predicted curve for the hygroscopicity properties of NaCl (line) from the Extended Aerosol Inorganic model (E-AIM) is shown for reference purposes.

Changes in equilibrium composition of aerosol droplets, principally the changes in water content, as a function of atmospheric conditions are likely to impact airborne transmission mechanisms through both changes in droplet size (affecting sedimentation and impaction rates) and microbe viability. Thus, an accurate understanding of the mass and heat transport accompanying the evaporation or condensation of water from aerosol droplets composed of respiratory fluids is increasingly recognized to be important to predict the risks in the airborne transmission of disease.[17-19] Aerosol droplets expelled when speaking, coughing, and sneezing evaporate to equilibrate with the surrounding atmosphere. The rate of mass and heat transfer to and from respiratory droplets is

determined by the conditions of the gas phase and the droplet composition, specifically the water activity of the solution phase.

Based on the equilibrium compositional measurements as a function of water activity presented in Figure S2, model predictions of evaporating artificial respiratory droplets into a wide range of RHs (30-90%) yield the time-dependent changes in size, solute concentration, surface-to-volume ratio and temperature suppression experienced by aerosol droplets in short periods (<30 s) after droplet generation as a function of the gas-phase RH (Figures S3, S4, S5 and S6). The kinetic simulations reported in *Supplemental Information* were obtained using the mass and heat transport equations from the Kulmala model[8] and the parametrization of density for each droplet solute described in detail in the *Supplementary Information*.

Probing Dynamics of Artificial Respiratory Droplets

The model predictions included in Figure S3, S4, S5 and S6 are for droplets composed of artificial saliva, artificial diluted (1:10) saliva, artificial sputum and artificial diluted (1:10) sputum, respectively. All the dynamic changes take place over a period of less than 30 s regardless of the ambient RH (<90%). Note that the simulations presented in this section are for relatively large droplets with initial sizes of 25μm radius (similar to those in a sneeze or in the articulation mode from the mouth when speaking).[20]

Specifically, rapid time-dependent changes in particle size during drying are shown in Figure 3a. where evaporation rates increase within decreasing RH and the final equilibrated radius are determined by the a_w in the droplets matching that of the gas phase RH.[3] The effect of droplet size alone on bacterial viability has been previously investigated being both directly proportional when solute concentrations and a_w are the same.[15] Further investigations also showed a significant impact of droplet size on bioaerosol survival.[21] Figure 3b shows the supersaturation of solutes within the droplets occurring over very short timescales (<5 s) which also depend on the RH, showing solute concentrations reaching over 800 g L^{-1} at the lowest RH level (30%). These supersaturated solute concentrations, ultra-viscous and glassy states[22] can potentially impact the viability of the airborne microorganisms.[23] The initial solute concentrations controls the shrinkage of the droplet while the surrounding gas-phase dictates the evaporation rates at which water evaporates. Indeed, the interface is a unique microenvironment in comparison to the droplet core with solute concentrations at the surface often evolving more rapidly and microbes unable to diffuse away from the surface as the surface boundary retracts. Further, mechanisms of loss of viability, such as exposure to atmospheric oxygen and ozone, direct solar radiation, and open-air factors (OAF),[24,25] may be more facile at the interface. Biological decay of microorganisms due to surface inactivation has been reported in various studies performed in shaking solutions and in aerosol droplets.[26]

The rate of inactivation seems to be dependent on the RH, salt concentrations, the protective effect of surface-active amino acids and the presence of air, and has been attributed to the extrusion of hydrophobic parts of the microorganisms into the air phase.[26-28] Benbough et al. demonstrated the toxicity of oxygen on airborne bacteria at low RH which was connected to the loss of bound structural water from the microorganism, producing changes in the reactivity of macromolecules (throughout free-radical formation) and, consequently, the inactivation of oxidative enzymes.[29,30] This makes the surface-to-volume ratio an important property of aerosols to consider when studying microbial survival. The surface-to-volume ratios of aerosols (<100 microns) is several orders of magnitude higher than those of macroscopic solutions.[17] As a result, microorganisms enclosed in aerosol droplets will spend a larger fraction of their time at the air-particle interface when compared to the bulk phase. Figure 3c shows kinetics simulations of the surface-to-volume ratio experienced by aerosol droplets as a function of the gas-phase RH. Finally, the temperature changes during the evaporative process undergone by the

droplets immediately after generation is shown in Figure 3d, reaching values up to 13K in less than 5 s at 30% RH.
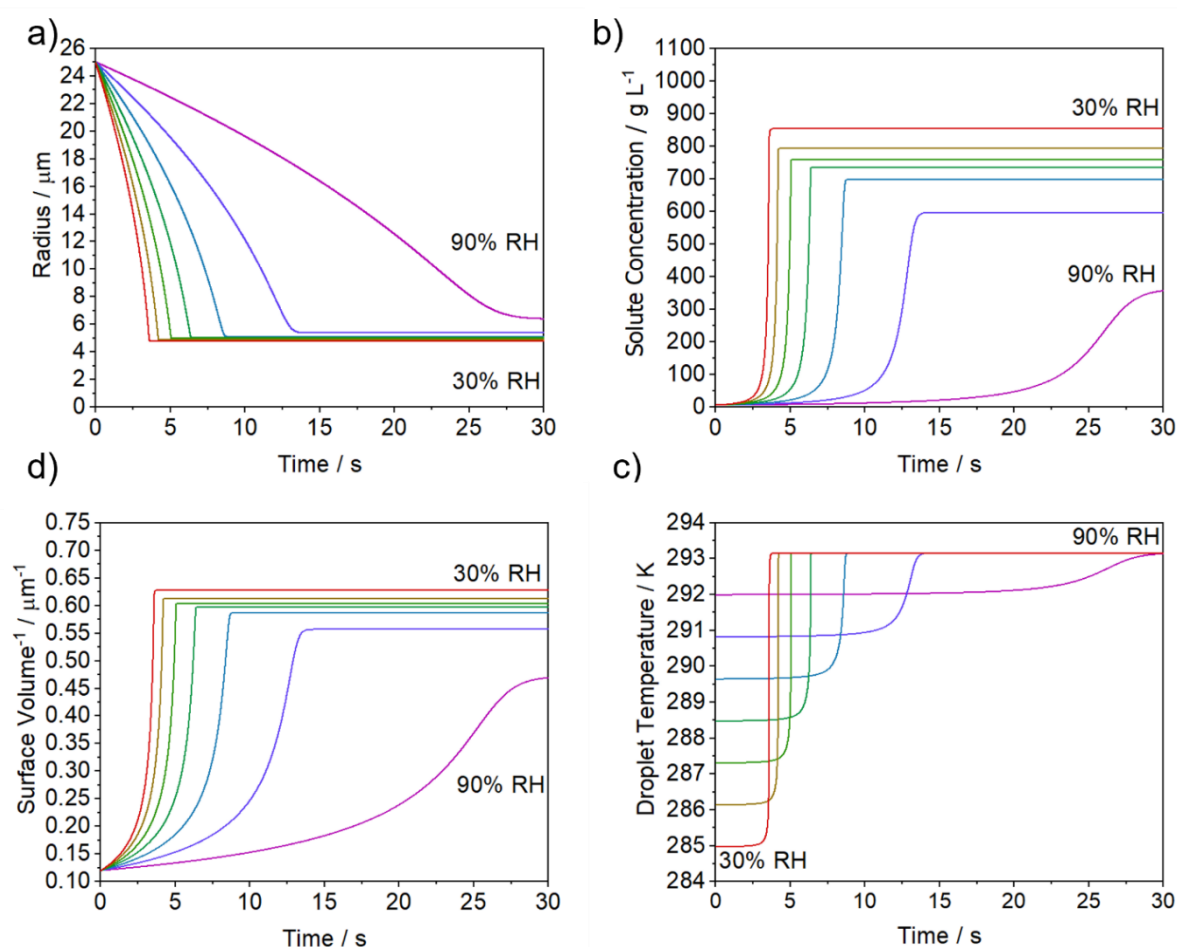

Figure S3. Modelled dynamics for artificial saliva droplets (neat concentration). Specifically, model results of the time-dependent (a) evaporating radius, (b) solute concentration, (c) surface-to-volume ratio and (d) temperature suppression for droplets equilibrating over an RH interval between 30 and 90% at 20℃. .

Evaporation on exhalation leads to rapid and dramatic changes in solute concentration, droplet size and even droplet temperature. Thus, aerosol particles can exhibit supersaturated states with solute concentrations higher than the solubility limit for macroscopic solutions, enhanced reactivity rates[31,32] and even unique phase behaviour[33] due to their chemical and physical characteristics. The kinetics of mass and heat transfer of the aerosol droplets will not only affect the viability of the airborne microorganisms but also the droplet lifetime in the aerosol phase (e.g., loss rates dues to sedimentation)[16] as well as their deposition in the respiratory system.[34,35] Therefore, it is critical to understand the impact that aerosol dynamics have on the transmission of airborne pathogens.
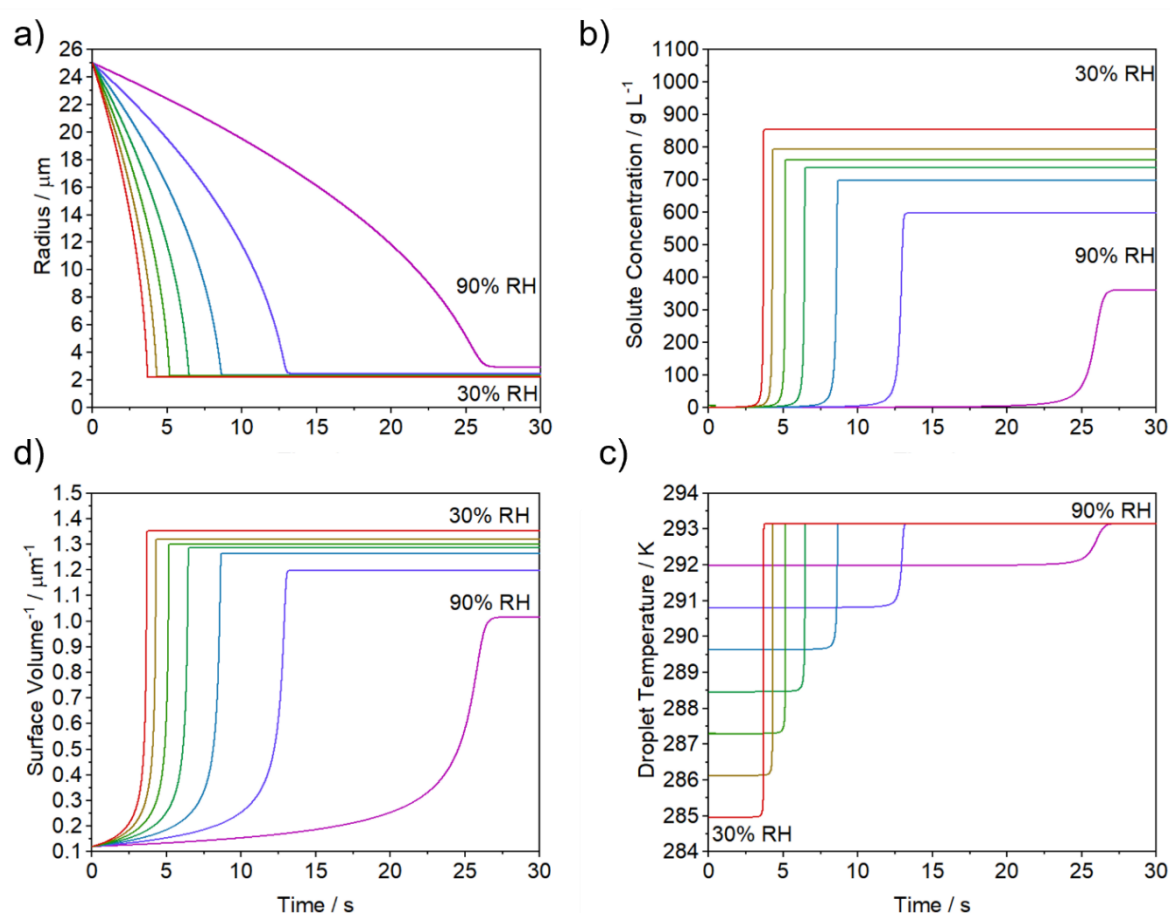
Figure S4. Modelled time-dependent dynamics for diluted artificial saliva droplets (1:10). (a) evaporating radius, (b) solute concentration, (c) surface to volume ratio and (d) temperature suppression for droplets equilibrating over a RH interval between 30 and 90% at 20°C.
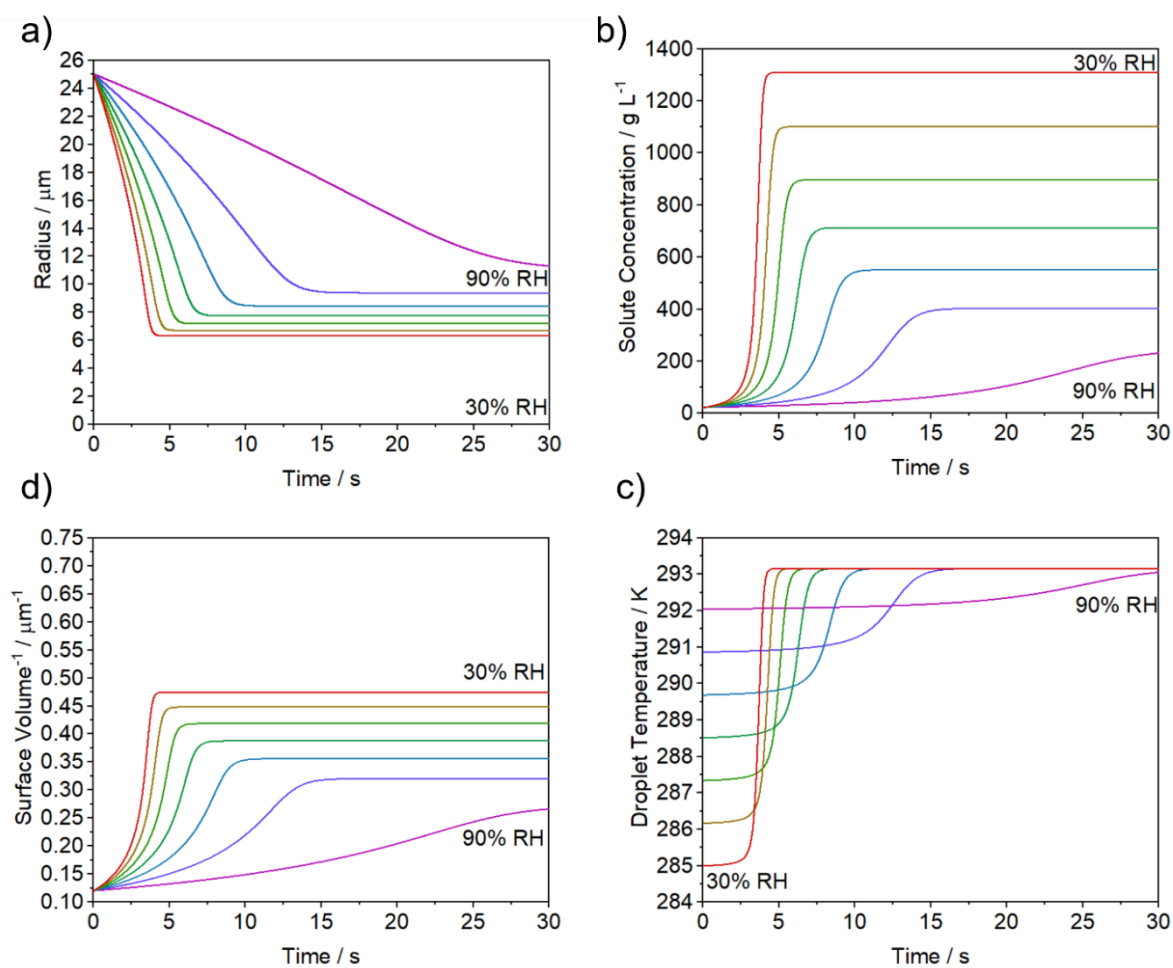
Figure S5. Modelled time-dependent dynamics for artificial sputum droplets. (a) evaporating radius, (b) solute concentration, (c) surface to volume ratio and (d) temperature suppression for droplets equilibrating over a RH interval between 30 and 90% at 20°C. **.**
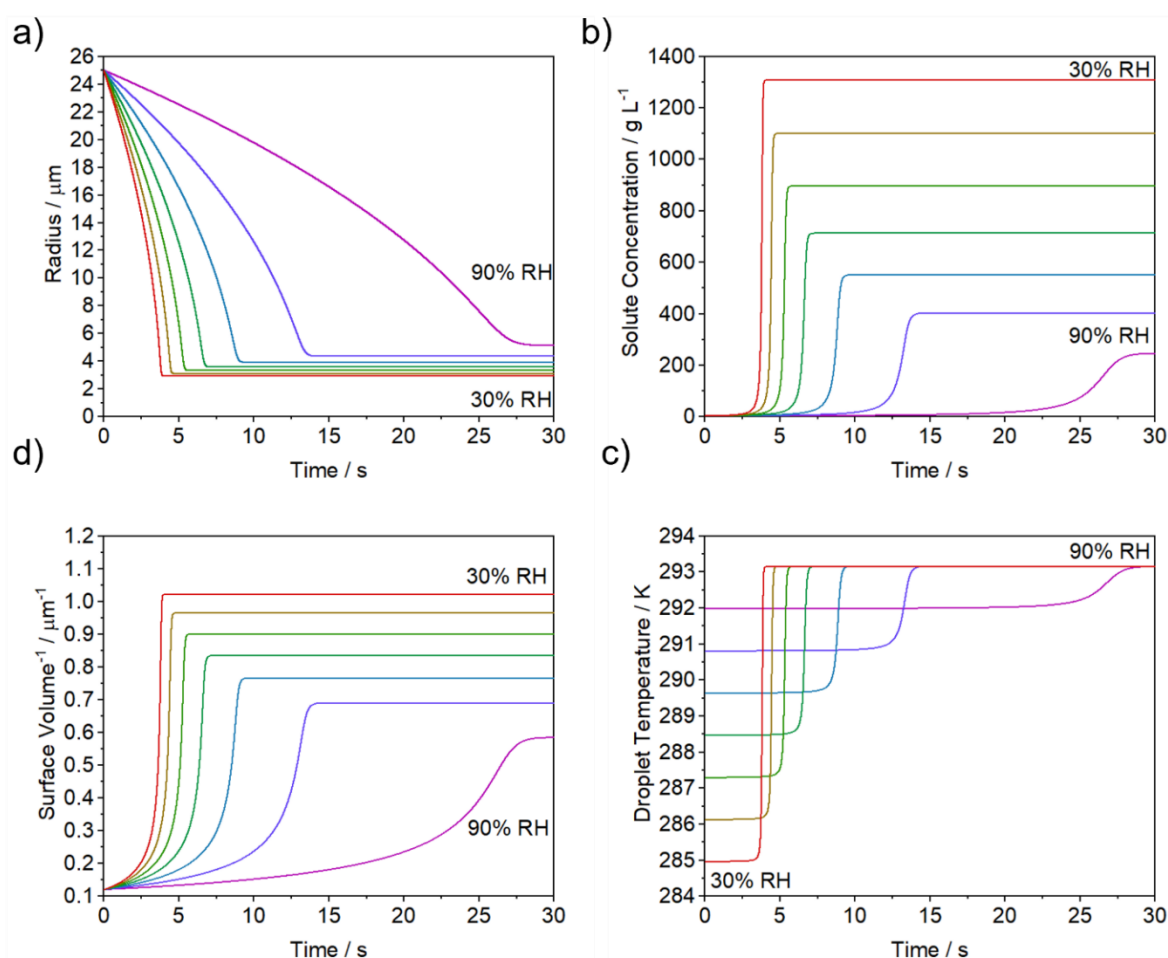
Figure S6. Modelled dynamics for diluted artificial sputum droplets (1:10). Specifically, model results of the time-dependent (a) evaporating radius, (b) solute concentration, (c) surface to volume ratio and (d) temperature suppression for droplets equilibrating over a RH interval between 30 and 90% at 20°C. **.**

Correlation Between Airborne Bacterial Longevity and Aerosol Physicochemical Properties

By coupling together the longevity data in Figure 1 with the physicochemical properties of the same aerosol particle types reported in Figure S2, we are able to explore whether there are fundamental parameters of aerosol that specifically affect bacteria viability. The viability of airborne *E. coli* MRE-162 at 600s of suspension as a function of six different physicochemical variables are shown in Figure S7: equilibrated droplet volume, the surface to volume ratio, equilibrate solute concentration, the concentration of salts at equilibrium, the equilibrated concentration of Na^+ and temperature suppression of the droplet when equilibrating with the gas-phase atmosphere. From all correlations, three (Figure S7A, Figure S7B and Figure S7F) reported a significant collective correlation (with α=0.05) for the five different particle compositions (e.g. diluted sputum, saliva, diluted saliva, LB broth and PBS) reporting R values of 0.631 for droplet volume, 0.626 for surface to volume ratio and 0.595 for droplet cooling with corresponding p-values of 0.006, 0.007 and 0.011 respectively. Besides, correlation coefficients were also calculated for other parameters not included in Figure S6, obtaining significant collective correlations also for evaporation rates, Peclet numbers, RH, final to initial volume ratio and surface area with R values of 0.607, 0.607, 0.589, 0.631 and 0.595 and p-values of 0.010, 0.010, 0.013 and 0.007, 0.012 respectively. The majority of these correlations relate to the evaporation dynamics

(e.g. evaporation rates, temperature cooling, etc) experienced by the aerosol particles as the reach equilibrium size in short timescales after generation, reflecting a delayed impact in survival over longer times in the aerosol phase (e.g. 600s) instead of after few seconds of suspension (e.g. 5 or 120 s). It is important to note that these processes will affect the final phase and morphology of the bioaerosol particles, determining the location of the microorganisms in the particles once equilibrated with the gas phase and, therefore, define the different degrees of exposure to open-air and other toxic factors they will experience.
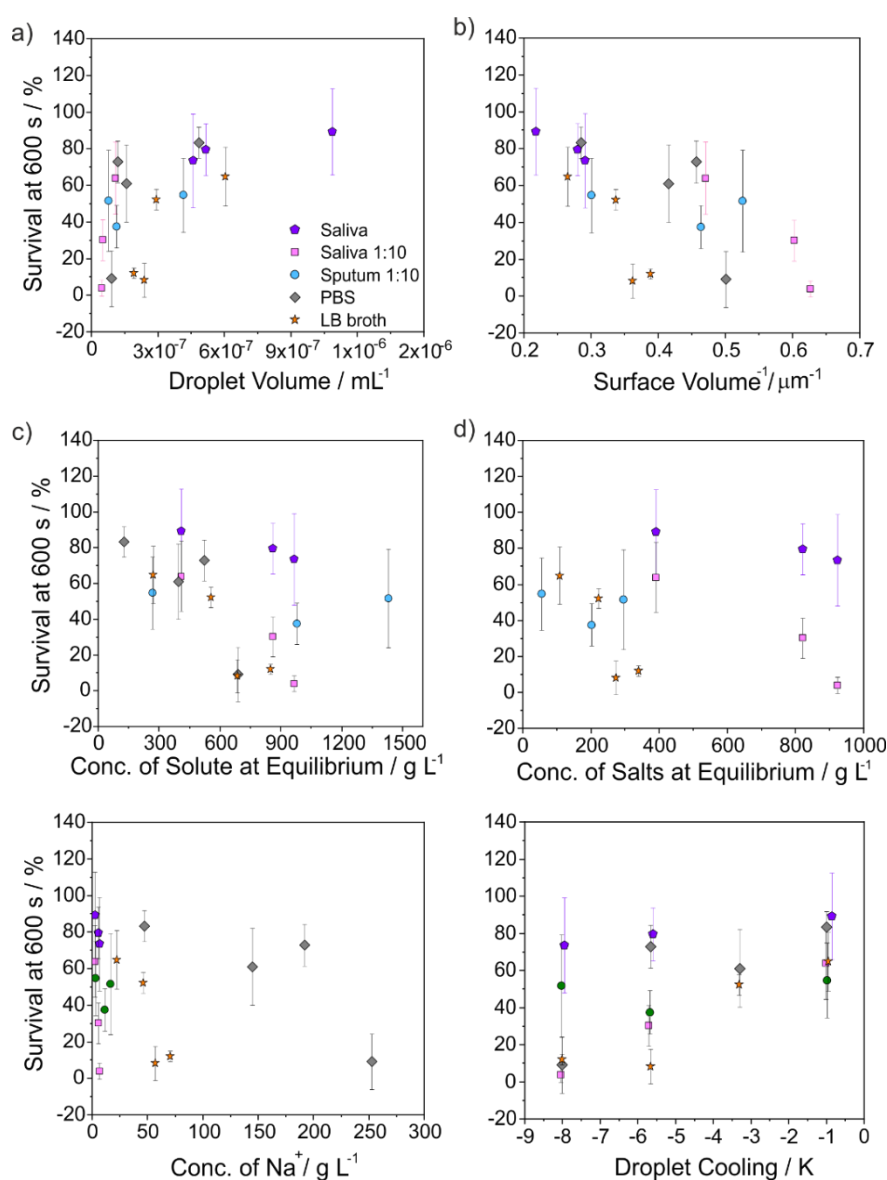

Figure S7. Correlations between bacterial survival and physicochemical changes in a) droplet volume at equilibrium, b) surface area to volume ratio, c) solute concentration at equilibrium, d) concentration of salts at equilibrium, e) concentration of Na+ at equilibrium and f) maximum droplet cooling for droplets of 5 different compositions evaporating into RHs of 30, 50, 70 and 90%. Note that in the case of Saliva, 1:10 Saliva and 1:10 Sputum the correlations at 70% RH are not reported. The droplet dynamics for all droplet composition were calculated using the mass-transfer kinetic model for droplets with an initial size of 25 ⌈m and an initial solute concentration of 25 g L^{-1} for LB broth, 9.59 g L^{-1} for PBS, 5.98 g L^{-1} for Saliva, 0.59 g L^{-1} for 1:10 Saliva and 2.12 g L^{-1} for 1:10 Sputum.
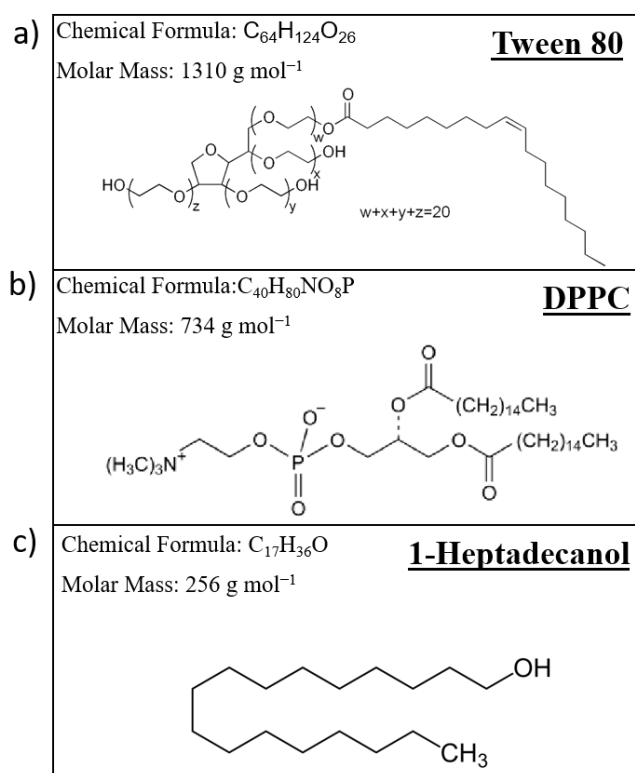
Surfactants

Figure S8. Chemical formulas, structures and molar masses of surfactants, a) Tween 80, b) 1,2-dypalmitoyl-rac-glycero-3-phosphocholine (DPPC) and c) 1-Heptadecanol.
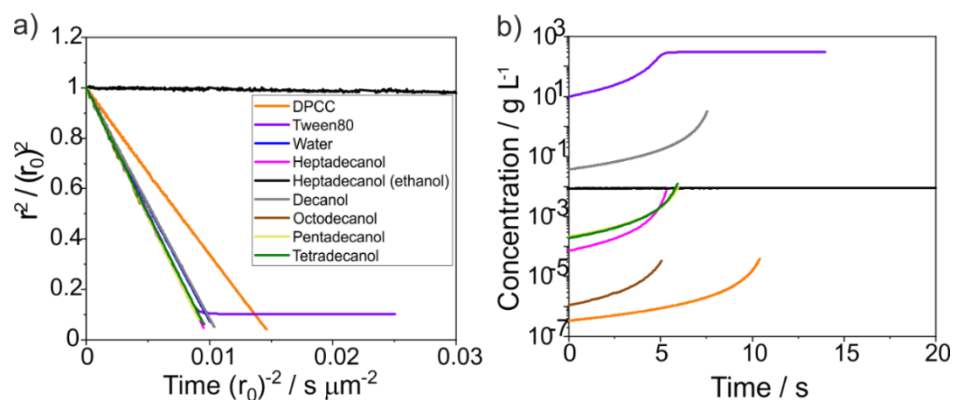

Figure S9. Physicochemical changes of water droplets containing various surfactants (a) Measured radii of a series of 7 saturated water solutions droplets containing different surfactants compared to that of pure water solution (light blue) and to that of heptadecanol dissolved in a 1:1 water-ethanol mixture (black) into the same conditions. (b) For the same droplets, change in the volume-average concentration as a function of time inferred from the experimental measurements of radii. Colours for the different water solution compositions under study: Orange, violet, magenta, green, navy blue, grey and brown – saturated water solutions with DPPC, Tween80, heltadecanol, decanol, octadecanol, pentadecanol and tetradecanol, respectively.

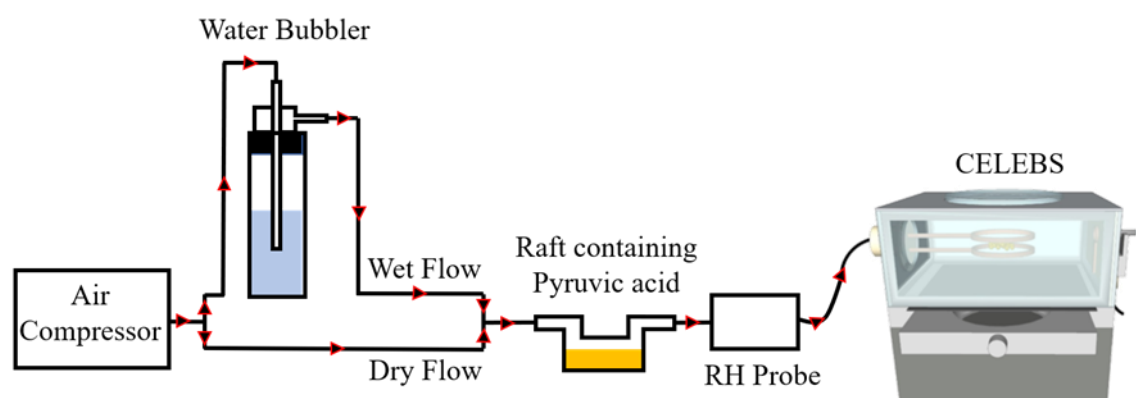**Proxy for Secondary Organic Aerosol**

Figure S10. Diagram of the gas flow set-up for pyruvic acid studies on bacterial viability.

Table S3. Equilibrium saturation concentrations of pyruvic acid in the aqueous phase as a function of the volume fraction of pyruvic acid introduced in the gas inlet at 30% RH.

Volume percentage of Pyruvic Acid in bubbler as an aqueous solution (% v/v)	Vapour pressure of pyruvic acid above equilibrated solution (atm)	Solution phase concentration of Pyruvic acid in the bubbler and equilibrated in the droplet (mol kg^{-1})
0	0.00	0.00
0.01	4.34×10^{-08}	0.01
0.1	4.34×10^{-07}	0.13
100	1.70×10^{-03}	527.55

References

1. Kirchner, S.; Fothergill, J.L.; Wright, E.A.; James, C.E.; Mowat, E.; Winstanley, C. Use of artificial sputum medium to test antibiotic efficacy against Pseudomonas aeruginosa in conditions more relevant to the cystic fibrosis lung. *J Vis Exp* **2012**, e3857, doi:10.3791/3857.

2. Woo, M.H.; Hsu, Y.M.; Wu, C.Y.; Heimbuch, B.; Wander, J. Method for contamination of filtering facepiece respirators by deposition of MS2 viral aerosols. *J Aerosol Sci* **2010**, *41*, 944-952, doi:10.1016/j.jaerosci.2010.07.003.

3. Rovelli, G.; Miles, R.E.H.; Reid, J.P.; Clegg, S.L. Accurate Measurements of Aerosol Hygroscopic Growth over a Wide Range in Relative Humidity. *The Journal of Physical Chemistry A* **2016**, *120*, 4376-4388, doi:10.1021/acs.jpca.6b04194.

4. Gregson, F.K.A.; Robinson, J.F.; Miles, R.E.H.; Royall, C.P.; Reid, J.P. Drying Kinetics of Salt Solution Droplets: Water Evaporation Rates and Crystallization. *The Journal of Physical Chemistry B* **2019**, *123*, 266-276, doi:http://10.1021/acs.jpcb.8b09584.

5. Haddrell, A.; Rovelli, G.; Lewis, D.; Church, T.; Reid, J. Identifying time-dependent changes in the morphology of an individual aerosol particle from its light scattering pattern. *Aerosol Sci Tech* **2019**, *53*, 1334-1351, doi:http://10.1080/02786826.2019.1661351.

6. Cai, C.; Miles, R.E.; Cotterell, M.I.; Marsh, A.; Rovelli, G.; Rickards, A.M.; Zhang, Y.H.; Reid, J.P. Comparison of Methods for Predicting the Compositional Dependence of the Density and Refractive Index of Organic-Aqueous Aerosols. *J Phys Chem A* **2016**, *120*, 6604-6617, doi:10.1021/acs.jpca.6b05986.

7. Davies, J.F.; Haddrell, A.E.; Reid, J.P. Time-Resolved Measurements of the Evaporation of Volatile Components from Single Aerosol Droplets. *Aerosol Sci Tech* **2012**, *46*, 666-677, doi:http://10.1080/02786826.2011.652750.

8. Kulmala, M.; Vesala, T.; Wagner, P.E. An analytical expression for the rate of binary condensational particle growth. *Proceedings of the Royal Society of London. Series A: Mathematical and Physical Sciences* **1993**, *441*, 589-605, doi:http://10.1098/rspa.1993.0081.

9.   Davies, J.F.; Haddrell, A.E.; Rickards, A.M.; Reid, J.P. Simultaneous analysis of the equilibrium hygroscopicity and water transport kinetics of liquid aerosol. *Anal Chem* **2013**, *85*, 5819-5826, doi:http://10.1021/ac4005502.

10.   Kreidenweis, S.M.; Koehler, K.; DeMott, P.J.; Prenni, A.J.; Carrico, C.; Ervens, B. Water activity and activation diameters from hygroscopicity data - Part I: Theory and application to inorganic salts. *Atmos. Chem. Phys.* **2005**, *5*, 1357-1370, doi:10.5194/acp-5-1357-2005.

11.   Baldelli, A.; Boraey, M.A.; Nobes, D.S.; Vehring, R. Analysis of the Particle Formation Process of Structured Microparticles. *Molecular Pharmaceutics* **2015**, *12*, 2562-2573, doi:10.1021/mp500758s.

12.   Nenninger, A.; Mastroianni, G.; Robson, A.; Lenn, T.; Xue, Q.; Leake, M.C.; Mullineaux, C.W. Independent mobility of proteins and lipids in the plasma membrane of Escherichia coli. *Mol Microbiol* **2014**, *92*, 1142-1153, doi:10.1111/mmi.12619.

13.   Clegg, S.L.; Brimblecombe, P.; Wexler, A.S. Thermodynamic Model of the System H+−NH4+−Na+−SO42-−NO3-−Cl-−H2O at 298.15 K. *The Journal of Physical Chemistry A* **1998**, *102*, 2155-2171, doi:10.1021/jp973043j.

14.   Fernandez, M.O.; Thomas, R.J.; Garton, N.J.; Hudson, A.; Haddrell, A.; Reid, J.P. Assessing the airborne survival of bacteria in populations of aerosol droplets with a novel technology. *J R Soc Interface* **2019**, *16*.

15.   Fernandez, M.O.; Thomas, R.J.; Oswin, H.; Haddrell, A.E.; Reid, J.P. Transformative Approach To Investigate the Microphysical Factors Influencing Airborne Transmission of Pathogens. *Appl Environ Microb* **2020**, *86*, e01543-01520, doi:http://10.1128/AEM.01543-20.

16.   Walker, J.S.; Archer, J.; Gregson, F.K.A.; Michel, S.E.S.; Bzdek, B.R.; Reid, J.P. Accurate Representations of the Microphysical Processes Occurring during the Transport of Exhaled Aerosols and Droplets (vol 7, pg 200, 2021). *Acs Central Sci* **2021**, *7*, 507-507, doi:http://10.1021/acscentsci.1c00220.

17.   Bzdek, B.R.; Reid, J.P.; Cotterell, M.I. Open questions on the physical properties of aerosols. *Communications Chemistry* **2020**, *3*, 105, doi:10.1038/s42004-020-00342-9.

18.   Nicas, M.; Nazaroff, W.W.; Hubbard, A. Toward understanding the risk of secondary airborne infection: emission of respirable pathogens. *J Occup Environ Hyg* **2005**, *2*, 143-154, doi:10.1080/15459620590918466.

19.   Haddrell, A.E.; Thomas, R.J. Aerobiology: Experimental Considerations, Observations, and Future Tools. *Appl Environ Microb* **2017**, *83*, e00809-00817, doi:http://DOI:10.1128/AEM.00809-17.

20.   Johnson, G.R.; Morawska, L.; Ristovski, Z.D.; Hargreaves, M.; Mengersen, K.; Chao, C.Y.H.; Wan, M.P.; Li, Y.; Xie, X.; Katoshevski, D.; et al. Modality of human expired aerosol size distributions. *J Aerosol Sci* **2011**, *42*, 839-851, doi:https://doi.org/10.1016/j.jaerosci.2011.07.009.

21.   Lighthart*, B.; Shaffer, B.T. Increased Airborne Bacterial Survival as a Function of Particle Content and Size. *Aerosol Sci Tech* **1997**, *27*, 439-446, doi:10.1080/02786829708965483.

22.   Power, R.M.; Simpson, S.H.; Reid, J.P.; Hudson, A.J. The transition from liquid to solid-like behaviour in ultrahigh viscosity aerosol particles. *Chemical Science* **2013**, *4*, 2597-2604, doi:10.1039/C3SC50682G.

23.   Yang, W.; Marr, L.C. Mechanisms by Which Ambient Humidity May Affect Viruses in Aerosols. *Appl Environ Microb* **2012**, *78*, 6781-6788, doi:10.1128/Aem.01658-12.

24.   de Mik, G.; de Groot, I. The germicidal effect of the open air in different parts of The Netherlands. *J Hyg (Lond)* **1977**, *78*, 175-187, doi:10.1017/s0022172400056072.

25.   Trouwborst, T.; de Jong, J.C. Mechanism of the inactivation of the bacteriophage T 1 in aerosols. *Appl Microbiol* **1972**, *23*, 938-941, doi:10.1128/am.23.5.938-941.1972.

26.   Trouwborst, T.; Kuyper, S.; de Jong, J.C.; Plantinga, A.D. Inactivation of some bacterial and animal viruses by exposure to liquid-air interfaces. *J Gen Virol* **1974**, *24*, 155-165, doi:10.1099/0022-1317-24-1-155.

27.   Kim, C.K.; Gentile, D.M.; Sproul, O.J. Mechanism of Ozone Inactivation of Bacteriophage f2. *Appl Environ Microbiol* **1980**, *39*, 210-218, doi:10.1128/aem.39.1.210-218.1980.

28.   Adams, M.H. Surface inactivation of bacterial viruses and of proteins. *J Gen Physiol* **1948**, *31*, 417-431, doi:10.1085/jgp.31.5.417.

29.   Benbough, J.E. Factors affecting the toxicity of oxygen towards airborne coliform bacteria. *J Gen Microbiol* **1969**, *56*, 241-250, doi:10.1099/00221287-56-2-241.

30.   Cox, C.S.; Baldwin, F. The toxic effect of oxygen upon the aerosol survival of Escherichia coli B. *J Gen Microbiol* **1967**, *49*, 115-117, doi:10.1099/00221287-49-1-115.

31.   Banerjee, S.; Gnanamani, E.; Yan, X.; Zare, R.N. Can all bulk-phase reactions be accelerated in microdroplets? *Analyst* **2017**, *142*, 1399-1402, doi:10.1039/C6AN02225A.

32.   Yan, X.; Bain, R.M.; Cooks, R.G. Organic Reactions in Microdroplets: Reaction Acceleration Revealed by Mass Spectrometry. *Angew Chem Int Ed Engl* **2016**, *55*, 12960-12972, doi:10.1002/anie.201602270.

33.   Reid, J.P.; Bertram, A.K.; Topping, D.O.; Laskin, A.; Martin, S.T.; Petters, M.D.; Pope, F.D.; Rovelli, G. The viscosity of atmospherically relevant organic particles. *Nat Commun* **2018**, *9*, 956, doi:10.1038/s41467-018-03027-z.

34.   Ng, C.S.; Chong, K.L.; Yang, R.; Li, M.; Verzicco, R.; Lohse, D. Growth of respiratory droplets in cold and humid air. *Physical Review Fluids* **2021**, *6*, 054303, doi:10.1103/PhysRevFluids.6.054303.

35.   Cheng, Y.S. Mechanisms of pharmaceutical aerosol deposition in the respiratory tract. *AAPS PharmSciTech* **2014**, *15*, 630-640, doi:http://10.1208/s12249-014-0092-0.